JOURNAL OF MATERIALS SCIENCE 23 (1988) 4027–4036

An evaluation of double-torsion testing of polymers by visualization and recording of curved crack growth

R. FRASSINE, T. RICCÒ, M. RINK, A. PAVAN
Dipartimento di Chimica Industriale e Ingegneria Chimica "G. Natta", Politecnico di Milano, Italy

The development and growth of the curved crack front in a double-torsion fracture-mechanics specimen is investigated by direct observation of crack propagation during the test. The crack front motion is analysed from a video-recording of the fracture test, and three distinct stages of crack propagation are identified. This work shows some of the requirements for the application of conventional double-torsion analysis to this test configuration: the material characteristic – critical strain energy release rate as a function of crack velocity – can be correctly obtained, provided that three steady-state conditions (static, kinematic and dynamic) are all fulfilled.

1. Introduction

Double-torsion (DT) testing is a useful experimental technique introduced in 1966 by Gerry [1] and subsequently applied by Kies and Clark [2]. It has been successfully used, in the last fifteen years, for the fracture mechanics characterization of many materials, such as ceramics [3–6], glass [7–9] and brittle or semi-brittle polymers [10–14].

Interest in the DT test is due to its experimental simplicity and the possibility of determining fracture resistance as a function of crack speed in rate-sensitive materials. The former characteristic is particularly attractive and advantageous if DT is compared to other test methods [9]: the test piece is a simple rectangular plate, and the only machining required (in addition to edge-notch milling) is side-grooving aimed at preventing crack wandering.

The four-point loading system applied at the notched end of the specimen (Fig. 1) generates a torsion on each of the two rectangular beams separated by the notch: a curved crack develops from the notch and runs through the specimen following the direction of the groove.

Under linear elastic conditions, the strain energy release rate, G, (kJ m^{-2}) can always be expressed in terms of specimen compliance, C (μm N^{-1}), as follows

$$G = \frac{P^2}{2}\frac{dC/da}{dA/da} \quad (1)$$

where P is the load (KN), a is the crack length from the load plane, measured at the lower edge of the specimen (mm) and A the crack surface are (mm^2). In order to derive the term (dC/da) for this test configuration, a conventional "pure torsion" analysis [15] has been satisfactorily applied. From that analysis, specimen compliance is expressed by

$$C = \frac{l^2}{k_1 \mu W B^3} a + C_0 \quad (2)$$

where l is the distance between the load points for a single beam (mm), k_1 a geometrical correction factor, μ the shear modulus (GPa), W the specimen width (mm), B the specimen thickness (mm) and C_0 the specimen compliance for $a = 0$ (μm N^{-1}) and P the load, which indicates the linear dependence of the compliance, C, on the crack length, a. Alternatively, the function $C(a)$ can, of course, be determined experimentally by direct measurement on a series of specimens with varying a.

If the crack profile does not change with crack extension, it can be shown that [16]

$$\frac{dA}{da} = B_c \quad (3)$$

where B_c is the thickness at the groove (mm).

The critical value of the strain energy release rate, G_c (kJ m^{-2}), can then be determined by measurement of the value of the load at fracture, P_c (kN) once the "calibration factor" (dC/da) has been determined. Combination of the theoretical result Equation 2 and Equations 1 and 3 gives us [4, 10, 17]

$$G_c = \frac{P_c^2}{2B_c}\frac{l^2}{k_1 \mu W B^3} \quad (4)$$

Once the geometrical parameters are assigned, Equation 4 directly relates G_c to P_c, so that G_c can simply be determined from the value of P_c, without needing to know a. Under general testing conditions, the crack may grow at a varying speed $\dot{a} = \dot{a}(t)$ (where $\dot{a}$ is the nominal crack velocity in mm sec^{-1}) and G_c and P_c will both vary during the test, since $G_c = G_c(\dot{a})$.

From the definition of specimen compliance, $C = x/P$, where x is the cross-head displacement (mm), the following expression of crack speed can immediately be derived

$$\dot{a} = \frac{\dot{x}}{P_c(dC/da) + C(dP_c/da)} \quad (5)$$

0022–246i/88 $03.00 + .12

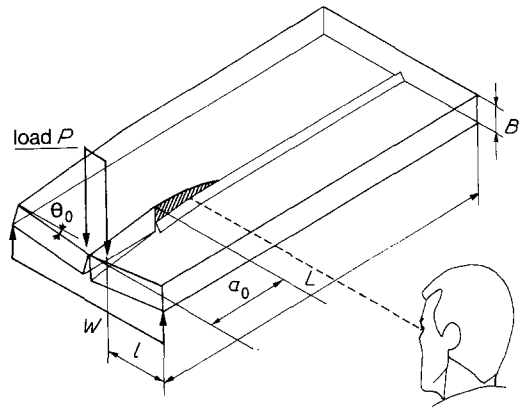

Figure 1 Geometry and loading arrangement of the double-torsion specimen, with crack growth as observed during tests.

If the fracture test is carried out in a displacement-controlled machine at constant cross-head speed, $\dot{x}$, and $G_c(\dot{a})$ is a monotonically increasing function of crack speed, $\dot{a}$, the constant P_c regime is in order, as shown by Leevers [18], and Equation 5 is simplified as follows

$$\dot{a} = \frac{\dot{x}}{P_c(dC/da)} \quad (6)$$

which predicts that a kinematic steady-state ($\dot{a}$ = constant) will parallel the dynamic steady-state (P_c = constant) (the limitation imposed on the $G_c(\dot{a})$ function of being monotonically increasing confines the applicability of Equation 6 to continuous crack propagation, excluding phenomena such as "stick–slip" propagation).

From Equations 4 and 6 it thus appears possible to derive the $G_c(\dot{a})$ characteristic of the material, with no need to measure a or $\dot{a}$ directly.

Some approximations limit the general validity of this analysis, however. Thus

(1) The two torsional beams are not ideally clamped at their ends, since the uncracked portion of the plate is compliant [16]; they also undergo a warping deformation [19].

(2) The coupling of the two beams generates a region of compressive stresses at the upper-inner side of the two beams, preventing them from overlapping [16].

(3) The stress distribution along the crack front is triaxial, and the principal stresses change in direction and magnitude with thickness [19–21].

(4) Linear compliance actually holds good only for the central portion of the crack length range [7, 20]: at both extremes, the compliance C against a curve shows upturns.

(5) From the curvature of the crack front, several complexities in interpretation arise, since crack velocity distribution along the crack front calls for some corrections of the G_c against $\dot{a}$ values calculated [18, 22–25].

(6) "Pure torsion" analysis assumes small deflections. Under this condition, the specimen compliance C can be determined from the expression $C = x/P$, as in Equation 2. When large deflections are reached, however, this relationship holds with approximation only, and has to be corrected [14, 26] as necessary.

The aim of this work is to re-examine some of the complexities in interpretation inherent in this test, in order to define better the requirements and limits of its application.

To this end, the entire crack-growth process was recorded by means of a video camera connected to a video recorder. The recording was then analysed by means of a computer: each frame sampled was digitized, processed, and printed out. Together with the load–time recording, this system thus permits coupled analysis of the kinematics and dynamics of the fracture process.

2. Experimental details

For the present investigation we used a polymeric material that is optically transparent and brittle under normal test conditions: cast sheets of a commercial polymethylmethacrylate were kindly supplied by Vedril S.p.A.

DT specimens were obtained from sheets varying in thickness between 3 and 12 mm; the in-plane dimensions of the samples were between 30 and 120 mm wide and 150 mm, or more, long. The specimens were edge-notched by means of a disc saw and side-grooved to a depth ($B - B_c$) of about 20% of plate thickness, B. The notch tip was then sharpened by forcing a razor blade into the material. For the test, the specimen is laid on two parallel rounded bars whose spacing can be varied. The load is applied at the upper side of the specimen by means of two small hemispheres (3 mm in radius and placed 13 mm apart), that move as one with the cross-head of a screw-driven Instron testing machine.

One side of the specimen was metallographically polished and the running crack was viewed perpendicularly to its plane through the polished face (Fig. 1): particular care was taken to avoid any optical distortion in crack growth monitoring.

The video recording system consists of a Ikegami CTC-6000 professional television camera, offering high resolution (800 lines) and high sensitivity (illuminance range: 1–100 luxes), connected to a Sony U-Matic VO-5800 PS 3/4″ standard video-recorder. The major features of this standard are high resolution of the output video signal (340 lines for the monochrome mode), a stable playback picture, and a very stable still picture; semi-frames are generated every 1/48 of a second. A high-resolution TV monitor (800 lines) was used to have real-time crack observation during the test. Since the resolution of the video picture is limited by the recorder's 340-line output, suitable optical lenses were used to provide sufficient magnification of the crack image. Each image can then be digitized, processed by computer, and printed out.

Crack growth shooting and load-recording were synchronized for subsequent quantitative correlation.

All the results given in this paper were recorded at room temperature and constant cross-head displacement rates, chosen on the basis of Equation 6, so as to maintain the crack speed, $\dot{a}$, constant under varying specimen dimensions.

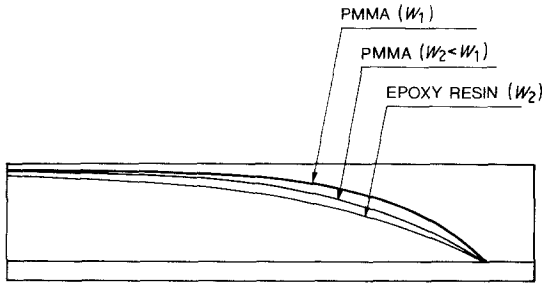

Figure 2 Crack front profiles for different materials and specimen widths.

3. Experimental results

This work can be divided into parts covering five topics. First ("crack front shape") we analyse the shape of the crack during its propagation following the direction of the groove; secondly ("statics"): the applicability of Equation 2 to specimens with different dimensions is verified; third ("kinematics") the development of the crack from the initial notch through the entire section and length of the specimen is investigated; fourth ("dynamics") by combining the experimental load–displacement curve and the simultaneously recorded crack growth development, we assess the limits for achieving the requisite steady-state regime; and fifth ("toughness measurement and test validation") the determination of material toughness via the theoretical Equation 4 is checked against the direct measurement of the specific fracture energy (dU/dA).

3.1. Crack front shape

Strain analysis of the double-torsion configuration has shown that both specimen geometry and material characteristics have an influence on crack front shape [18, 24]. Our experimental results show that both specimen thickness, B, and width, W, affect crack front shape, in agreement with the findings of several authors: Fig. 2 indicates the comparable effect of specimen width and material (PMMA, rubber-modified epoxy resin) on crack shape, in agreement with Stalder and Kausch's findings [24].

By contrast, cross-head rate (or crack speed), in the range of 1 to 200 mm min^{-1}, was found to have no influence on the shape of the crack front profile, as stated also by Stalder and Kausch.

The effect of variations in side-groove depth ($B - B_c$) was especially investigated in this work, in order to check the theoretical dependence of crack shape on B_c, resulting from previous analyses [18, 24]. It was found that the crack front profile has the same shape irrespective of B_c, for specimens of a given thickness, B, and width, W. Fig. 3 shows an example of this invariance: the pictures taken during crack propagation show the crack front profile on three specimens 12 mm thick and varying groove depth ($B - B_c$) = 2.5, 4 and 5.5 mm respectively (Fig. 3a). In Fig. 3b, the same profiles are redrawn with reference to the base line of the groove, given the same "nominal" crack length, a. In agreement with Stalder and Kausch's observations [24], attempts to superimpose these profiles by normalization in different coordinate axes (x, y), (x/B, y/B), (x/B_c, y/B_c) are in vain.

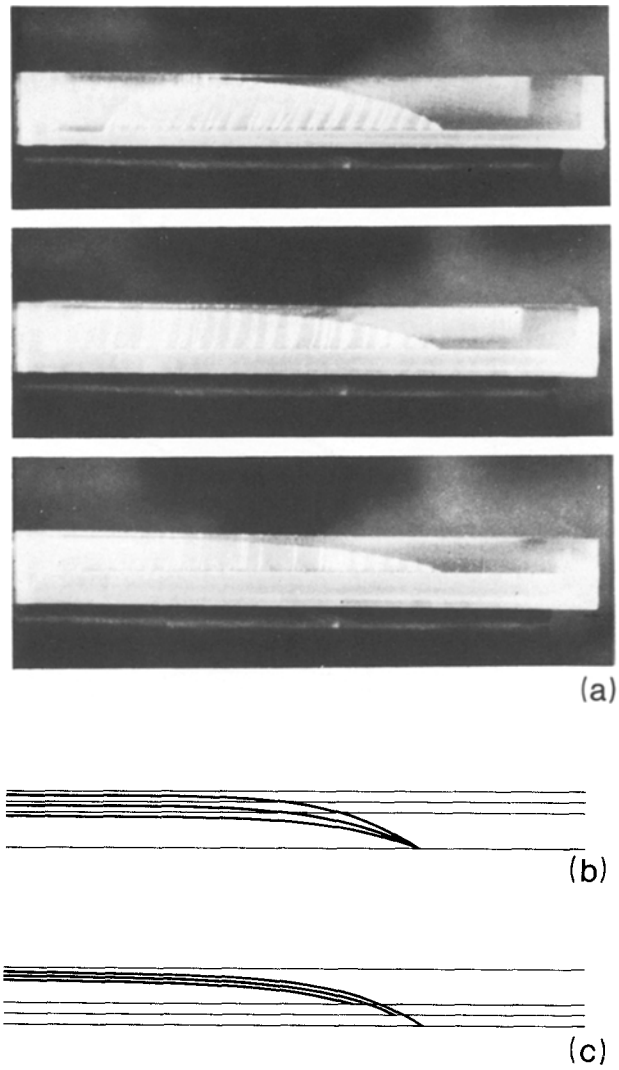

Figure 3 Effect of side-groove depth on crack shape. (a) Pictures taken during crack propagation on three specimens with different groove depths. (b) Crack profiles do not superimpose if referred to the base-line of the grooves, while they do (c) if referred to the opposite (ungrooved) side.

When the same profiles are referred to the opposite (ungrooved) side of the specimens, however, they appear superposable by a simple horizontal shift (Fig. 3c).

This result indicates that the stress and strain distributions determining the shape of the crack front are not affected by grooves of whatever depth, in agreement with Tseng and Berry's results [19]. The strain analyses [18, 24] appear to be in disagreement with our observations, because the theoretically derived hyperbolic shape of the curved crack explicitly depends on B_c. In Leevers's analysis, in fact, the hyperbolic function is calculated as

$$y = \frac{B_c^2 S}{x} + K_0 \qquad (7)$$

where S is a "shape factor" that depends on specimen geometry and material and K_0 a constant. Since the shape of the crack profile depends on the product $B_c^2 S$, S ought to be proportional to B_c^{-2} for the theory to be able to account for the present experimental observations. The analytical relationships given by Leevers and Williams [25] state a complex dependence of S on

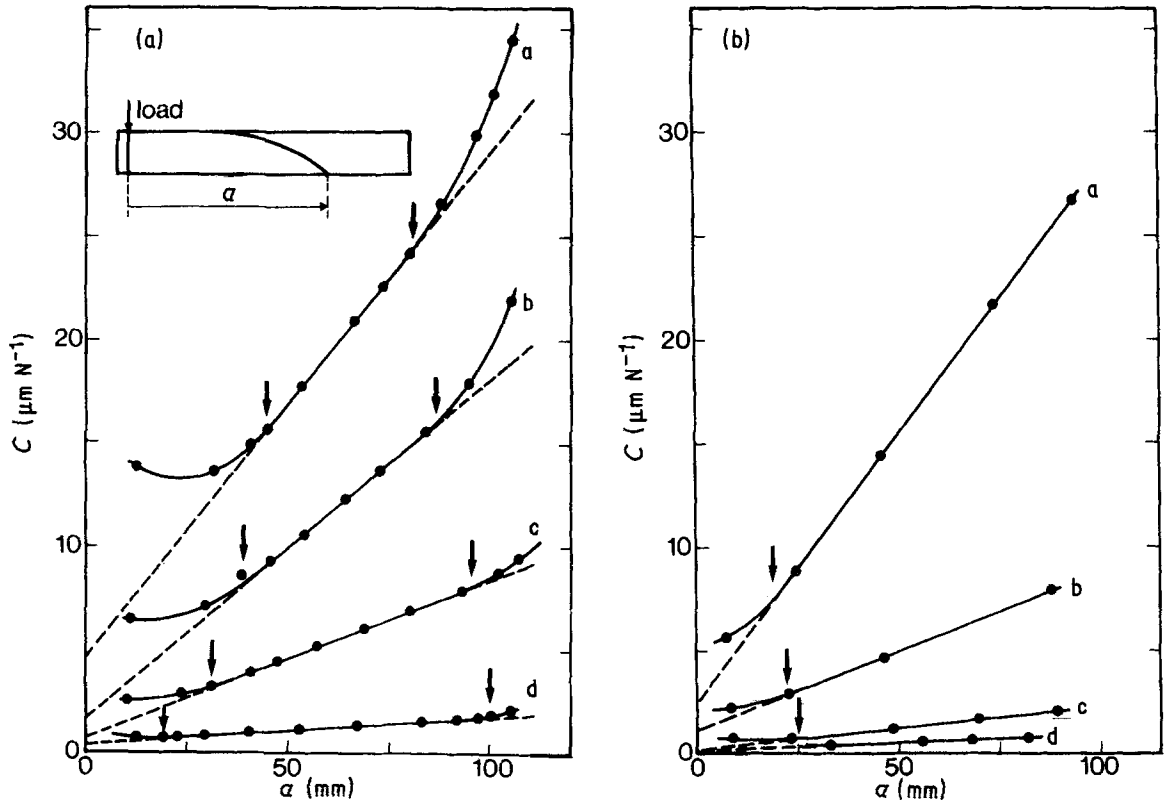

Figure 4 Specimen compliance, C, plotted against crack length, a, for (a) different specimen widths (a 106 mm, b 82 mm, c 52 mm, d 26 mm) and (b) thicknesses (a 3 mm, b 5 mm, c 8 mm, d 12 mm). Arrows indicate the linear compliance range.

B_c, i.e.

$$S = \frac{1}{Q}\coth\left(Q\frac{(L-a)}{B_c}\right) \tag{8}$$

where

$$\frac{1}{Q} \equiv \left(\frac{\pi}{6c}(1+\nu)\frac{2B_c^4}{k_1 WB^3}\right)^{-1/2} \tag{8'}$$

and L is the specimen length (mm), ν the Poisson's ratio, and c an adjusting factor introduced to account for the increased compliance of a finite crack path width. In Stalder and Kausch's analysis, the crack shape is given as

$$y = FM/x \tag{9}$$

where F is a material and M is a geometry-dependent function. Since M is directly related to B_c^{-1}, this theory is at variance with our experimental results.

3.2. Statics

Static measurements of the specimen compliance, C, as a function of "nominal" crack length, a, were carried out for different specimen widths, W, and thicknesses, B; different crack lengths were obtained by letting the crack propagate to different extents from a straight notch of constant length $a_0 = 10$ mm. The resulting plots (Fig. 4) always show deviations from linearity at the two ends of the crack length range explored: the linear compliance characteristic of the test is verified over a range of crack lengths that increases as specimen width (Fig. 4a) and thickness (Fig. 4b) decreases.

A tentative explanation of this experimental finding can be given in simple qualitative terms; for crack lengths less than about $W/2$, the two specimen halves are too short to be thought of as twisting in "pure torsion" and theoretical analysis becomes invalid; for crack lengths longer than $(L - W/2)$, on the other hand, the uncracked portion of the plate becomes more like a bar (perpendicular to crack growth direction) than a plate, behaving as a more compliant constraint for the two torsion beams.

Deviations from linear compliance can also be influenced by thickness, because of the curved crack: the full development of its profile through the specimen's thickness, from the initial straight notch, progressively modifies the geometry of the two twisting beams. Because of this, the range of linearity is reached with longer cracks in thicker specimens (Fig. 4b).

The experimental slope of the linear portion of these curves, (dC/da), was then compared with the theoretically predicted value of $[(dC/da)\mu]$, Equation 1, as shown in Fig. 5, the agreement is good.

From the least square fitting of these data, a value of 1.37 GPa is obtained for the shear modulus μ,

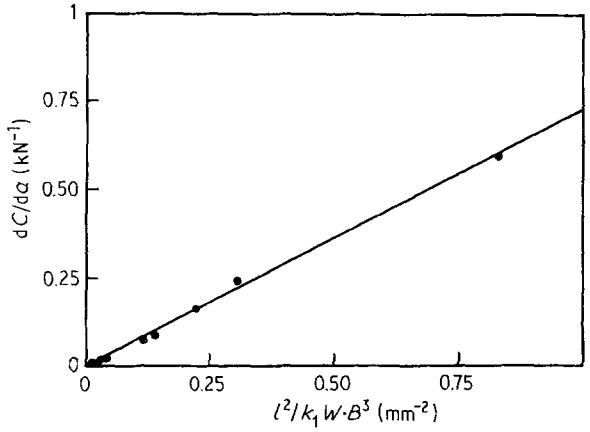

Figure 5 Values of compliance derivatives from data of Fig. 4, plotted against the calculated values of $[(dC/da)\mu]$ (see text).

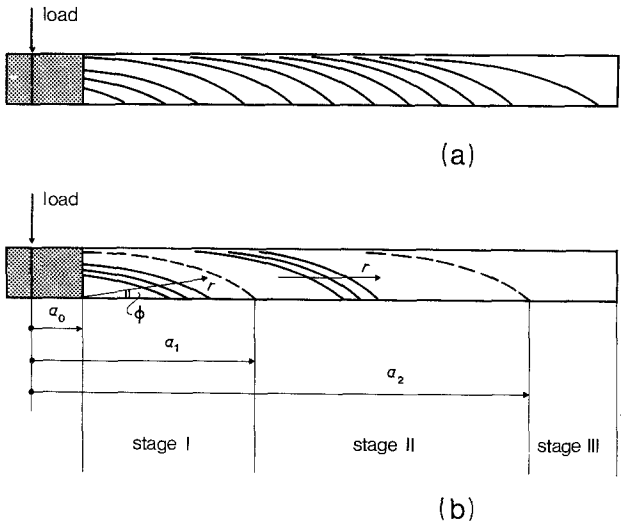

Figure 6 (a) Crack fronts during crack propagation (time between two crack fronts = 3 sec). (b) Identification of different stages of crack propagation.

which is quite close to the storage shear modulus $\mu' = 1.48$ GPa obtained at 1 Hz, 25° C for the same material.

While the analytical relationship, Equation 1, appears to be complied within the specimen size range experimentally examined, its application remains impaired by uncertainty as to the value of the shear modulus μ to be used, as pointed out by Stalder [27]: in fact, μ is strongly dependent on strain rate in most polymers, and the strain rate effectively applied in the DT configuration is difficult to determine exactly. It would, therefore, seem always to be advisable to have accurate experimental calibration of the compliance derivative, (dC/da), preferably obtained at the displacement rate to be used in the DT fracture test.

3.3. Kinematics

Three distinct stages are generally observed in crack growth (Fig. 6): first, the development of the curved crack front from the initial straight notch, through the entire thickness of the specimen; second, the "solid" translation of the developed profile of the crack front along the grooved, longer axis of the plate; third, the final abrupt break, which is an end effect that will not be considered here any further.

Detailed analysis of the video pictures shows that, even in the first stage of crack growth, the profile of any subsequent crack front comes from the same "master" curve as that observed in the second stage: in the first stage, however, the solid translation of the curve occurs in a direction tilted at an angle ϕ to the longer axis of the plate (Fig. 6b). In all the experimental tests carried out in the course of the present investigation, the angle ϕ was between 4° and 7°, while B_c was varied between 9.5 and 6.5 mm, B was maintained constant at 12 mm, and W was varied between 36 and 92 mm.

A correct approach to the kinematic description of crack growth calls for the classification of three different speeds (Fig. 7): the "nominal" crack speed $\dot{a}$ along the lower edge of the specimen; the "local" speed $\dot{\xi}$ (mm sec^{-1}) at a point P of the crack front,

Figure 7 Diagram showing the three different speeds considered for the description of crack propagation.

directed as its normal ξ; the translational speed of the crack profile, $\dot{r}$ (mm sec^{-1}).

Crack motion analysis shows that in stage I $\dot{r}$ is a constant, but is different from $\dot{a}$ in both value and direction, while in stage II $\dot{r}$ coincides with $\dot{a}$, and stationary crack propagation takes place. The speed distribution $\dot{\xi}$(P) along the crack front varies with time in stage I, until it reaches its definitive form at the beginning of stage II, as shown in Fig. 8, remaining invariant thereafter. From the distribution $\dot{\xi}$(P), a mean value can, of course, readily be evaluated. According to Pollet and Burns [23], the mean crack velocity, V, (mm sec^{-1}) can also be calculated from the nominal value of crack speed, $\dot{a}$, via Equation 10

$$V = \left(1/B_c \int_0^{B_c} \sin \alpha^{1/m} \, dx\right)^m \dot{a} \qquad (10)$$

where α is the radial coordinate [23] and m the crack growth exponent. The translational velocity of the "master" profile ($\dot{r} = \dot{a}$ in stage II) was found to be dependent on geometrical parameters (W, B, B_c), as predicted by the theoretical analysis, Equation 6.

During the development of the crack front in stage I, the fracture surface area, A, (cm^2) does not increase linearly with crack extension, a, as it does in stage II: Equation 3 and the subsequent analysis are then applicable to stage II only.

Starting from this observation, it is possible to model the crack movement by simple geometrical considerations.

In agreement with Leevers [18] and Stalder and Kausch [24], we assume that the crack profile is described by a hyperbolic function, with the general equation

$$v = H/u \qquad (11)$$

where H is a constant, when the coordinate system (u, v) is taken as indicated in Fig. 9a.

In stage II, where the crack front has reached its full development, it is more convenient to refer to coordinate axes (x, y) placed in physically significant positions, i.e. root of the notch and upper side of the specimen, as indicated in Fig. 9b; with this transformation, the equation of the hyperbolic curve becomes

$$y = \frac{H}{B_c}\left(\frac{x - B_c}{x}\right) + (a - a_0) \qquad (12)$$

where $H = B_c^2 S$ in Leevers' notation.

In stage I, where the crack front has not yet reached the upper side of the test specimen, the shape of its profile can again be described by Equation 12, provided that it is referred to a coordinate system (x', y') moving as one with the crack front in a direction, r, tilted at the angle ϕ with respect to the y axis, as shown in Fig. 9c, i.e.

$$y' = B_c S\left(\frac{x' - B_c}{x'}\right) + (a_1 - a_0) \qquad (12')$$

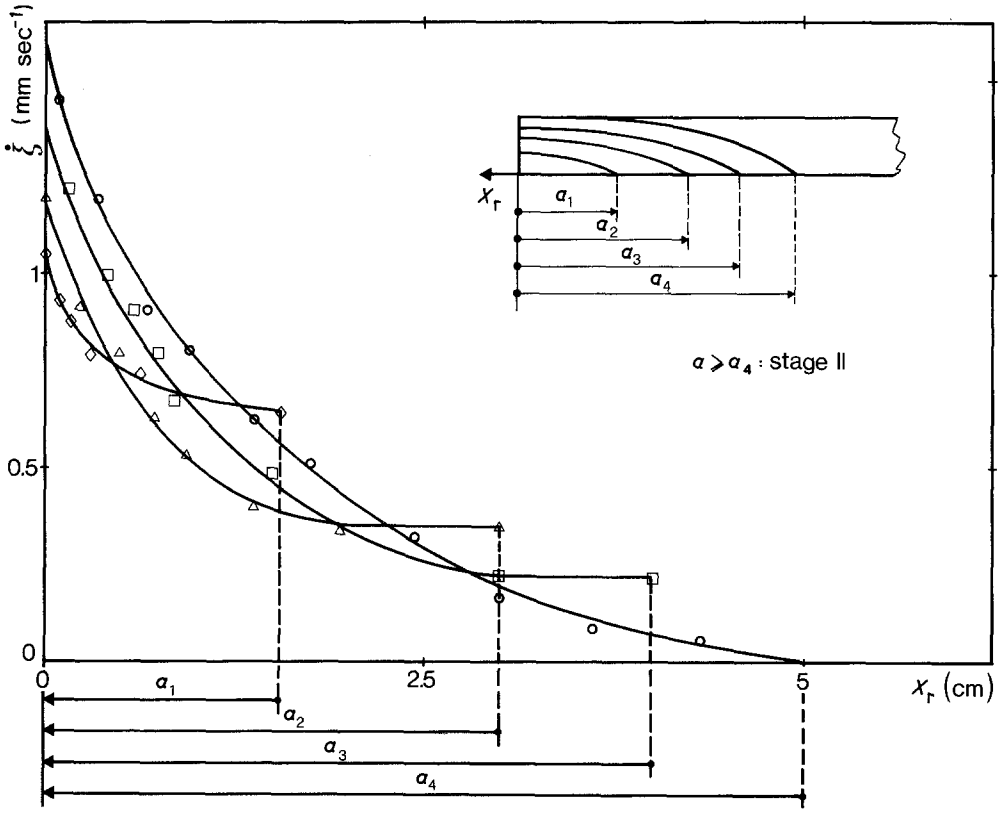

Figure 8 Distribution of local crack velocities along the crack profile, for different crack extensions. The origin of the x_r axis is taken at the intersection of each crack front with the lower edge of the specimen.

At the end of stage I ($a = a_1$), when the crack front reaches the upper side of the test specimen, the two reference systems (x', y') and (x, y) are superposed and Equation 12 and 12′ coincide.

The fracture surface area, A, (shaded in Fig. 9c) can then be calculated as a function of crack length, $a \leqslant a_1$, from the equation

$$A_I(a) = \text{MNPQ-RNPQ} = \overline{MN} \times \overline{MQ} - \int_{\overline{0'N}}^{\overline{0'P}} x' dy'$$

$$= (a - a_0)(B_c - \overline{00'} \sin \phi) - \int_{\overline{00'}\cos\phi}^{(a-a_0)+\overline{00'}\cos\phi} \times [SB_c^2/(a_1 - a_0) + SB_c - y'] dy' \quad (13)$$

By comparison, the fracture surface area in stage II (for $a \geqslant a_1$) can be obtained by integration of Equation 3, giving us

$$A_{II}(a) = B_c(a - a_0) + \text{constant.} \quad (14)$$

From this analysis the value a_1 of the crack length at the transition from stage I to stage II appears to be a function of the shape factor S, of the specimen thickness at the groove, B_c, and of the angle ϕ. Assuming continuity of the two expressions Equations 13 and 14 and of their derivatives at the transition from stage I to stage II, the value of a_1 can be predicted by solving the equation obtained by equating the two derivatives, once S, B_c and ϕ are known.

The resulting plot A against a is shown in Fig. 10 for both stages I and II: a comparison with the experimental data, obtained by measuring the fracture area of each crack length directly from the video pictures, shows good agreement. The stage I–stage II transition was here found at $a_1 = a_0 + 42$ mm.

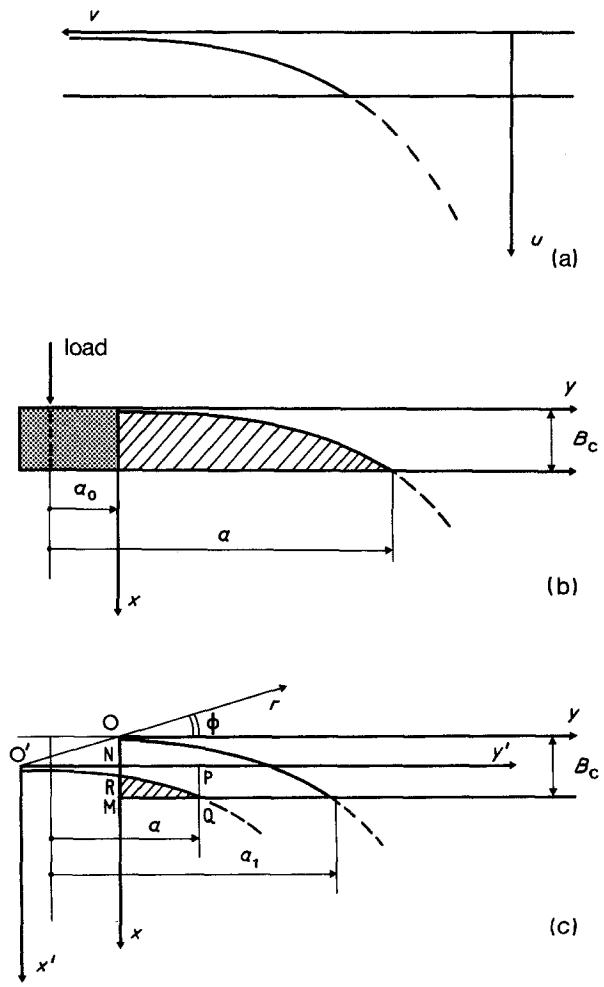

Figure 9 Illustration of the different coordinate systems considered for the analytical description of crack development and growth, as described in the text.

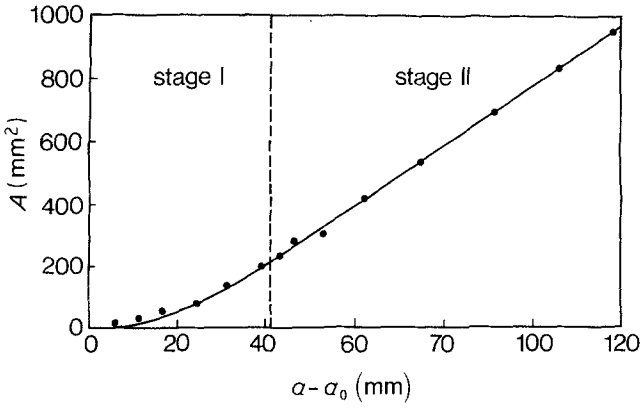

Figure 10 Fracture surface area as a function of crack length: comparison between experimental data (points) and calculated values via Equations 13 and 14 (full-line) (B_c = 9.5 mm, ϕ = 5°, S = 0.8).

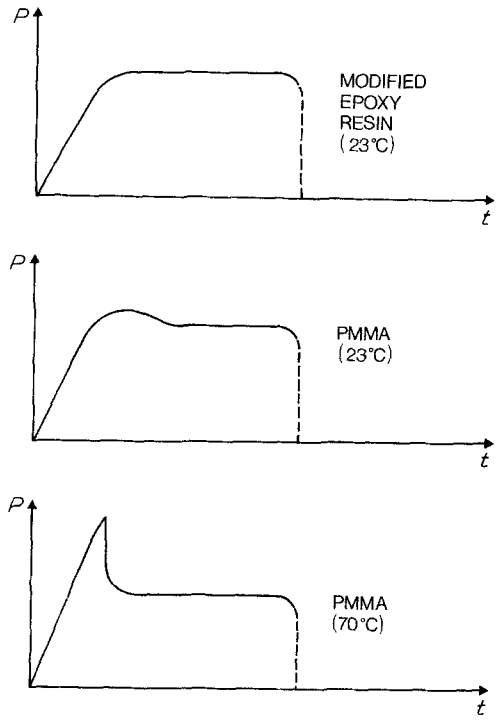

Figure 11 Load–time records (arbitrary units) observed in double-torsion tests for different materials and test temperatures.

3.4. Dynamics

A few typical load–time records are observed in DT tests, by varying the material, temperature, and displacement rate (Fig. 11).

Under conditions of continuous crack propagation, the dynamic steady-state (P_c = constant) can be reached beyond an initial transient in the load–time trace, provided a sufficient length is given to the test specimen.

In Fig. 12 the load–time record for PMMA at room temperature is compared with the corresponding crack speed diagram, drawn from the video-tape record. At first, the load, P, rises almost linearly with time (or displacement) till the crack starts to grow (beginning of stage I). Then the load–time curve bends and reaches a maximum, while the crack speed increases up to a constant value (beginning of stage II), as predicted by Virkar and Johnson [28]; however, the load keeps decreasing in stage II before coming to a "plateau". In the end (stage III) the load drops rapidly, while the crack accelerates up to the final break.

It is worth noting that the dynamic steady-state condition (P_c = constant) is reached in stage II, somewhat later than the static condition dC/da = constant and the kinematic condition $\dot{a}$ = constant. This result is consistent with the more general analysis

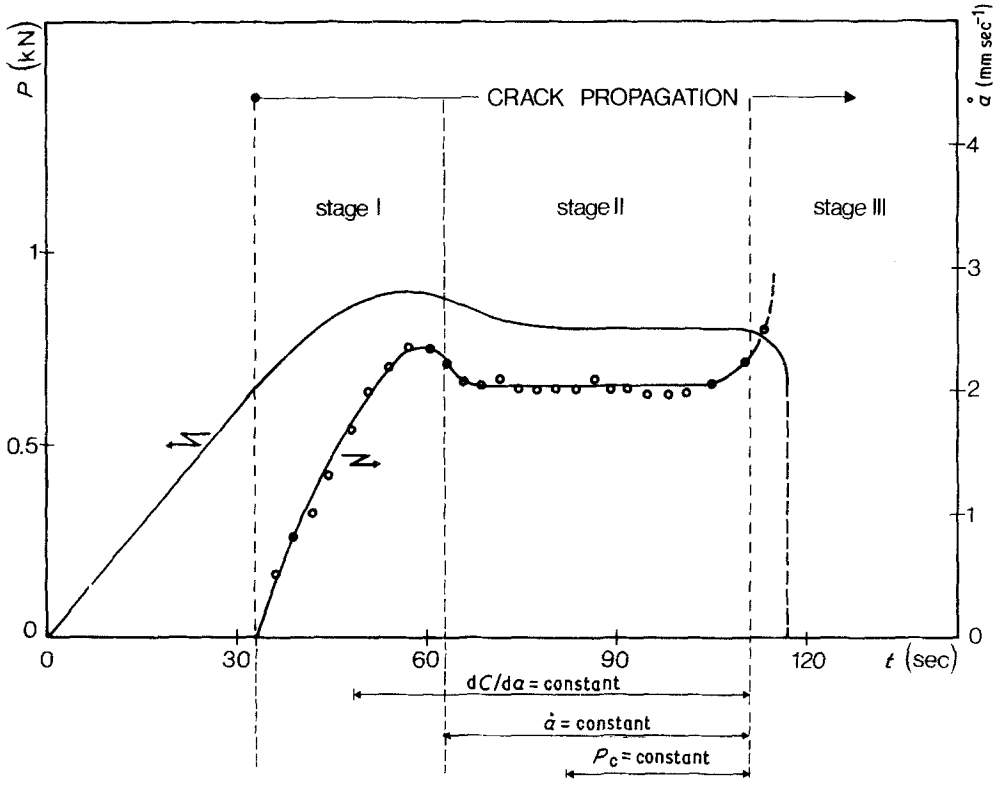

Figure 12 Load, P, and nominal crack velocity, $\dot{a}$, plotted against time during a typical double-torsion test. The intervals within which the three steady-state conditions (static, kinematic and dynamic) occur are also shown.

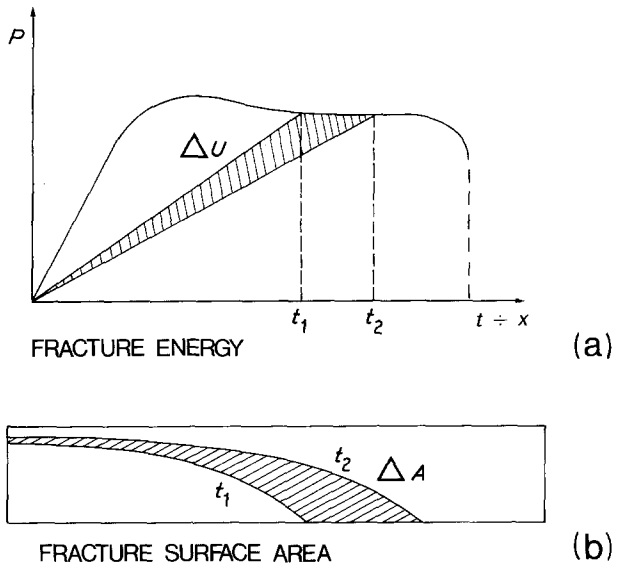

Figure 13 (a) Fracture energy, ΔU, released during a time interval ($\Delta t = t_2 - t_1$), and (b) the corresponding fracture surface area, ΔA, considered in calculating G_c from its definition (Equation 16).

based on Equation 5, from which it appears that P_c needs not be constant to have $\dot{a}$ = constant, when $\dot{x}$ and dC/da are constant.

As already pointed out, if toughness is a monotonically-increasing function of crack speed (as it is for PMMA under the test conditions we adopted), the dynamic steady-state regime is in order, since any change in P_c will be self-correcting according to Equations 4 and 5. Integration of Equation 5 under the conditions prevailing in stage II produces

$$P_c = \frac{\dot{x}}{\dot{a}}\left(\frac{dC}{da}\right)^{-1} + D_0\left[C_0\left(\frac{dC}{da}\right)^{-1} + a\right]^{-1} \quad (15)$$

where D_0 is a constant of integration. The first term is constant in stage II, coinciding with the steady-state value of the critical load (see Equation 6), while the second term governs the variation of P_c with a: the load P_c is thus expected to approach its steady-state value asymptotically.

All the load–time records reported in Fig. 11 appear to follow this behaviour: their differences have not been interpreted, however.

3.5. Toughness measurement and test validation

From the force–displacement curve and the video recordings of the fracture surface during the test, an average critical strain energy release rate, G_c, at whatever stage of crack growth, a, can be determined directly from the definition

$$G_c = \frac{dU}{dA} \quad (16)$$

The value of the energy increment (ΔU) spent on an extension ΔA of the fracture surface area during a time interval ($\Delta t = t_2 - t_1$) can be obtained from the load–time record, as shown in Fig. 13a, if linear elastic behaviour is assured. For the same time interval, the corresponding crack surface area increment, ΔA, can be directly measured from the two videograms taken at instant t_1 and t_2 (Fig. 13b). The linear elastic assumption for measuring the fracture energy increment is justified here, since the load was observed to vary linearly and reversibly with displacement during loadings and unloadings carried out while the crack is not propagating.

TABLE I Comparison of toughness results

Evaluation method	G_c ($J m^{-2}$)
a Equation 16	410
b Equation 4	516
c Equation 4 + LD*	464
d Equation 4 + CFC†	625
e Equation 4 + LD* + CFC†	563

*Correction for large deflections.
†Correction for crack front curvature.

The value of G_c so determined is an average of the energy $G_c(\dot{\xi})$ non-uniformly absorbed along the curved crack front because of the distribution in local crack velocity $\dot{\xi}$ [25]. The curves G_c plotted against $(a - a_0)$ obtained are thus not crack resistance curves (R curves) of the material, that do not vary with test configuration, but may, at the most, be regarded as crack resistance curves of the material *in this test.*

Comparison of one such curve (Fig. 14a) with the plot of the corresponding mean crack velocity, V, calculated from Equation 10 (Fig. 14b) shows some similarity. In stage I, G_c varies with crack extension, as a consequence of the variation in the distribution of local crack velocities; the average velocity, V, also varies, together with the nominal crack speed, $\dot{a}$. In stage II, however, the crack profile is fully established, so that the distribution of local crack velocities remains constant with crack propagation. The variation of G_c with crack extension, observed in the initial part of stage II, is thus unexpected; it parallels the variation of the load (Fig. 12), which remains to be interpreted.

In Table I, the "plateau" value of G_c, determined directly from the definition (Equation 16), is compared with values obtained with the compliance method (Equation 4) and corrected for large deflections (LD) according to Leevers [26]* and/or for the crack-front-curvature (CFC) according to the same author [18].

Results obtained according to evaluation methods a, b and c are in fact average values of G_c along the crack front where G_c varies, due to the distribution in local crack velocity, $\dot{\xi}$; by contrast, results d and e are values corrected for that distribution and refer to a crack velocity equal to the nominal crack speed, $\dot{a}$. Strictly speaking, then, results d and e are not comparable with results a, b and c. Comparison of results b and d, and c and e shows the increase in the G_c value brought about by correction for the crack front curvature; this result is expected, since the nominal crack

*The toughness correction factor, depends, naturally, on the deflection, x (Fig. 3 in [26]). For the present evaluation, the mean value of the deflection over the range in which P_c = constant was considered.

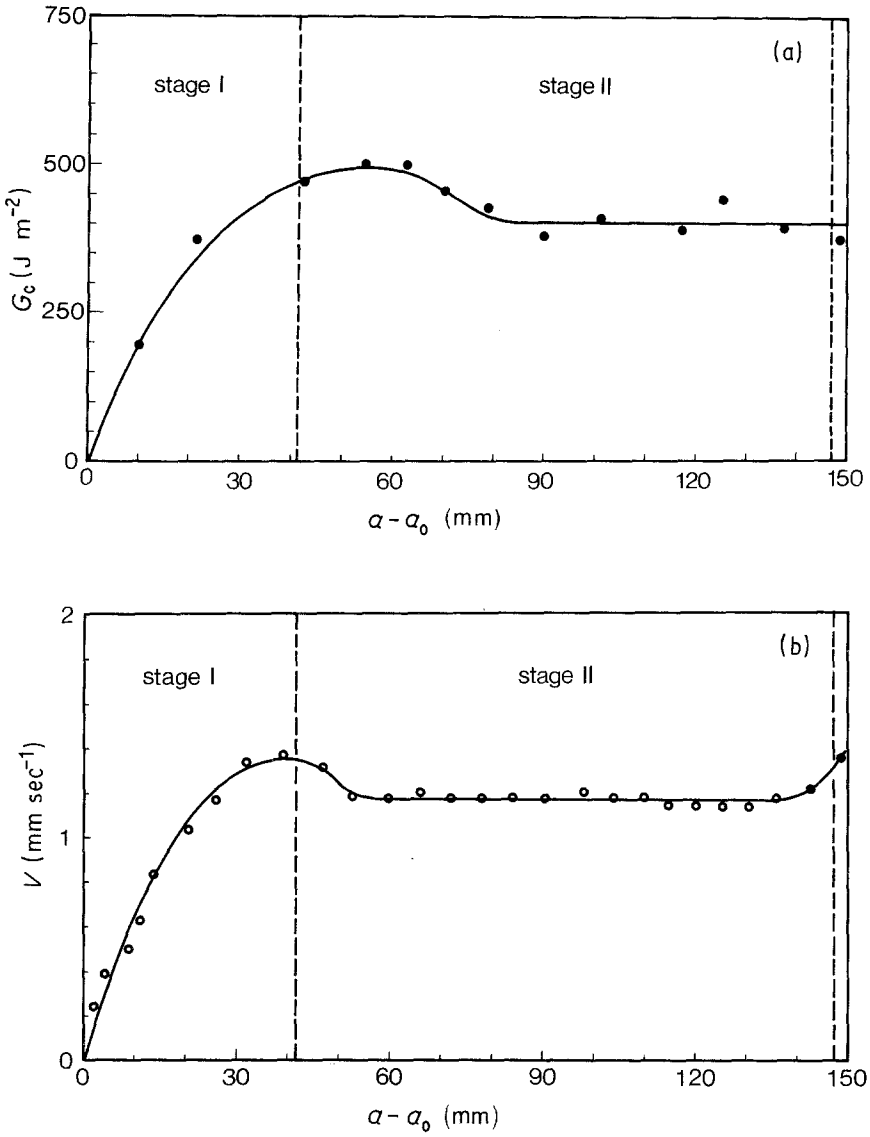

Figure 14 (a) Strain energy release rate, G_c, resulting from Equation 16 and (b) mean crack velocity, V, resulting from Equation 10 plotted against crack length, during the three stages of crack propagation.

speed, $\dot{a}$, is larger than any actual velocity $\dot{\xi}$ in the distribution $\dot{\xi}(P)$, and the CFC correction assumes G_c to be an increasing function of crack speed.

Comparison of results b and c shows, by contrast, the reducing effect of the LD correction, which is a purely geometrical one. Furthermore, comparison of results b, c and a shows that the LD correction (b → c) brings the value evaluated for G_c to fair agreement with the value obtained by direct application of the toughness definition; a 12% discrepancy still remains to be accounted for, however.

4. Conclusions

The theoretical predictions based on the "compliance analysis" (Equations 1–4) turn out to be confirmed with a satisfactory degree of precision, both on the static and the dynamic side. The various approximations made in that analysis and referred to here in the Introduction, do not appear to limit its validity for purposes of the practical application of this test. To this end, the steady-state fracture regime must indeed be achieved – and this happens only when the three conditions dC/da = constant (static), $\dot{a}$ = constant (kinematic) and P_c = constant (dynamic) are all fulfilled. The extent of the transient stage to be overcome before the complete steady-state regime is achieved depends on such factors as the shape of the crack profile, the angle ϕ of the profile slant translation in stage I, the material characteristics, and the test conditions. The present investigation shows that the crack can grow considerably before the steady-state is achieved and care must be taken to provide sufficient specimen length for the purpose.

Acknowledgements

This investigation is based on experimental observations and results collected in the course of a few year's research activity. Most of the experimental work was done by R.F. for his degree in Chemical Engineering [29], and part of it was presented at the 6th European Conference on Fracture [30]. Subsequent developments are part of research being done by R.F. in partial fulfilment of the requirements for his Research Doctorate in Materials Engineering.

The authors are grateful to MPI, Rome, for awarding R.F. a scholarship, and to CNR, Rome (Progetto Finalizzato Chimica Fine e Secondaria) for financial support.

References

1. D. J. GERRY, PhD Thesis, University of Vermont (1966).
2. J. A. KIES and A. B. J. CLARK, in "Fracture 1969" (Proceedings of the 2nd International Conference on Fracture, Brighton, 1969), edited by P. L. Pratt (Chapman and Hall, London, 1969) p. 483.
3. A. G. EVANS, *J. Mater. Sci.* **7** (1972) 1137.
4. *Idem., Int. J. Frac.* **9** (1873) 267.
5. R. W. DAVIDGE, J. R. McLAREN and G. TAPPIN, *J. Mater. Sci.* **8** (1973) 1699.
6. K. R. McKINNEY and H. L. SMITH, *J. Amer. Ceram. Soc.* **56** (1973) 30.
7. D. K. SHETTY and A. V. VIRKAR, *ibid.* **61** (1978) 93.
8. B. J. PLETKA, E. R. FULLER Jr, B. G. KOEPKE, ASTM STP 678 (edited by S. W. Freiman) (American Society for Testing and Materials, Philadelphia, 1979) p. 19.
9. F. P. CHAMPOMIER, ASTM STP 678 (edited by S. W. Freiman) (American Society for Testing and Materials, Philadelphia, 1979) p. 60.
10. P. W. R. BEAUMONT and R. J. YOUNG, *J. Mater. Sci.* **10** (1975) 1334.
11. R. J. YOUNG and P. W. R. BEAUMONT, *Polymer* **17** (1976) 717.
12. J. C. POLLET and S. J. BURNS, *Int. J. Frac.* **13** (1977) 775.
13. D. C. PHILLIPS, J. M. SCOTT and M. JONES, *J. Mater. Sci.* **13** (1978) 311.
14. P. J. HINE, R. A. DUCKETT and I. M. WARD, *ibid.* **19** (1984) 3796.
15. S. P. TIMOSHENKO and J. N. GOODIER, in "Theory of Elasticity" (McGraw-Hill Book, New York, 1970) p. 309.
16. E. R. FULLER Jr, ASTM STP 678 (edited by S. W. Freiman) (American Society for Testing and Materials, Philadelphia, 1979) p. 3.
17. G. P. MARSHALL, L. H. COUTTS and J. G. WILLIAMS, *J. Mater. Sci.* **9** (1974) 1409.
18. P. S. LEEVERS, *ibid.* **17** (1982) 2469.
19. A. A. TSENG and J. T. BERRY, *J. Press. Vess. Tech.* **101** (1979) 329.
20. G. G. TRANTINA, *J. Amer. Ceram. Soc.* **60** (1977) 338.
21. B. HINDIN, *Engng. Frac. Mech.* **19** (1984) 21.
22. A. V. VIRKAR and R. S. GORDON, *J. Amer. Ceram. Soc.* **58** (1975) 536.
23. J. C. POLLET and S. J. BURNS, *ibid.* **62** (1979) 426.
24. B. STALDER and H. H. KAUSCH, *J. Mater. Sci.* **17** (1982) 2481.
25. P. S. LEEVERS and J. G. WILLIAMS, *ibid.* **20** (1985) 77.
26. P. S. LEEVERS, *J. Mater. Sci. Lett.* **5** (1986) 191.
27. B. STALDER, PhD Thesis, Ecole Polytechnique Fédérale de Lausanne (1985).
28. A. V. VIRKAR and D. L. JOHNSON, *J. Amer. Ceram. Soc.* **59** (1976) 197.
29. R. FRASSINE, PhD Thesis, Politecnico di Milano, Italy (1984).
30. R. FRASSINE, T. RICCÒ, M. RINK and A. PAVAN, in "Fracture Control of Engineering Structures" (Proceedings of the 6th European Conference on Fracture, Amsterdam, June 1986) edited by H. C. von Elst and A. Batter (EMAS Ltd., Warley, West Midland, 1986), Vol. III, p. 2037.

Received 7 September 1987
and accepted 28 April 1988